Journal of Photochemistry and Photobiology A: Chemistry 262 (2013) 7–13

Contents lists available at SciVerse ScienceDirect

Journal of Photochemistry and Photobiology A: Chemistry

journal homepage: www.elsevier.com/locate/jphotochem

Optimization of photocatalytic performance of TiO_2 coated glass microspheres using response surface methodology and the application for degradation of dimethyl phthalate

Wenjun Jiang[a], Jeffrey A. Joens[a], Dionysios D. Dionysiou[b], Kevin E. O'Shea[a,*]

[a] Department of Chemistry and Biochemistry, Florida International University, Miami, FL 33199, USA
[b] Environmental Engineering and Science Program, University of Cincinnati, Cincinnati, OH 45221-0012, USA

ARTICLE INFO

Article history:
Received 21 January 2013
Received in revised form 22 March 2013
Accepted 14 April 2013
Available online 23 April 2013

Keywords:
Advanced oxidation
Photocatalysis
FTIR
Response surface methodology
Dimethyl phthalate remediation

ABSTRACT

Hollow glass microspheres coated with photocatalytic TiO_2 (HGM-TiO_2), recently became commercially available and have the distinct advantages of easy separation and recovery after treatment. With this in mind, we determined the optimum conditions for hydroxyl radical generation from HGM-TiO_2 photocatalysis using response surface methodology (RSM). The hydroxyl radical yield and its average generation rate are critical parameters for practical applications of TiO_2 photocatalysis. In this study, terephthalic acid was used as a hydroxyl radical trap because of the selective formation of the readily detectable hydroxyl radical adduct, 2-hydroxy terephthalic acid. Three independent variables, including loading of HGM-TiO_2, concentration of terephthalic acid and irradiation time, were investigated. The 3D response surface graphs of hydroxyl radical yield and average hydroxyl radical generation rate indicated that optimum conditions of loading of HGM-TiO_2, concentration of terephthalate acid and irradiation time were 8.0 g/L, 4.0 mM, and 20 min, respectively. Under these optimized conditions, we measured the photocatalysis employing HGM-TiO_2 for the remediation of dimethyl phthalate (DMP), as a representative compound for problematic phthalate acid esters. HGM-TiO_2 photocatalysis leads to the rapid destruction of DMP and there is a linear correlation between the DMP destruction and hydroxyl radical production. The results of our study demonstrate RSM can be used to readily determine the optimal conditions for hydroxyl radical production and the subsequent treatment of target compounds may be correlated to the hydroxyl radical production during HGM-TiO_2 photocatalysis.

1. Introduction

Access to clean water is a global problem and one of the primary causes of human health problems worldwide [1]. TiO_2 photocatalysis is an attractive method for the purification of water, due to its abilities to effectively degrade a tremendous variety of toxins and pollutants [2]. The degradation processes are initiated at the surface of TiO_2 [3]. When TiO_2 is photoexcited by photons with energy equal to or greater than the band gap, an electron is promoted from the valence band to the empty conduction band, resulting in an electron–hole pair. Electron–hole pairs can recombine or migrate to the surface and react with the adsorbed species on TiO_2 surface. The process can generate a variety of reactive oxygen species (ROS), including hydroxyl radical, hydrogen peroxide, singlet oxygen, and superoxide anion radical. Among the ROS, hydroxyl radical is generally responsible for the degradation during UV TiO_2 photocatalysis in aqueous solution [4,5]. The processes initiated during TiO_2 photocatalysis are represented in Eqs. (1)–(8). Hydroxyl radical is capable of reacting with most organic compounds and many inorganic compounds often at nearly diffusion controlled rates. Hydroxyl radical is a powerful electrophile and reacts with organic substances mainly by the addition to double and triple bonds, and aromatic rings, hydrogen-atom abstraction from $C_{(sp3)}$—H bonds, and electron transfer pathways [6]. Since the performance of TiO_2 photocatalysis for water treatment processes is highly dependent on hydroxyl radical, it is critical to evaluate and optimize experimental conditions for maximizing hydroxyl radical generation during TiO_2 photocatalysis.

$$TiO_2 + h\nu \rightarrow h^+_{VB} + e^-_{CB} \quad (1)$$

$$e^-_{CB} + O_2 \rightarrow O_2^{\bullet -} \quad (2)$$

Abbreviations: 2-HTA, 2-hydroxy terephthalic acid; ANOVA, analysis of variance; DMP, dimethyl phthalate; FTIR, Fourier transform infrared spectroscopy; HGM-TiO_2, hollow glass microspheres coated with photocatalytic TiO_2; ROS, reactive oxygen species; RSM, response surface methodology; TA, terephthalic acid.

* Corresponding author. Tel.: +1 305 348 3968; fax: +1 305 348 3772.
E-mail address: osheak@fiu.edu (K.E. O'Shea).

1010-6030/$ – see front matter © 2013 Elsevier B.V. All rights reserved.
http://dx.doi.org/10.1016/j.jphotochem.2013.04.008

$$2O_2^{\bullet -} + 2H_2O \rightarrow H_2O_2 + 2OH^- + O_2 \quad (3)$$

$$H_2O + h^+_{VB} \rightarrow {}^\bullet OH + H^+ \quad (4)$$

$$OH^- + h^+_{VB} \rightarrow {}^\bullet OH \quad (5)$$

$$H_2O_2 + e^-_{CB} \rightarrow OH^- + {}^\bullet OH \quad (6)$$

$$TiO_2 + h\nu + 3O_2 \rightarrow TiO_2 + {}^1O_2 \quad (7)$$

$$^\bullet OH + \text{toxin} \rightarrow \text{oxidation product} \quad (8)$$

In an attempt to improve the performance of UV TiO_2 photocatalysis, a variety of TiO_2 materials have been developed, including surface modification [7], TiO_2 films [8], doped TiO_2 [9], TiO_2 nanotubes [10], porous TiO_2 microspheres [11] and microspheric cores covered with TiO_2 shell/film [12]. Among these means, microspheric cores covered with nano- or micro-sized shells are novel fabricated composite materials and have received significant attention [13]. As an important composite material, HGM-TiO_2, recently became commercially available and has the major advantages of easy separation and recovery. Thus, HGM-TiO_2 is promising for use in industrial wastewater treatment plants and gaseous pollutants reduction, due to unique properties, such as low density (0.22 g/cm^3), buoyancy, and transparency to visible light. However, detailed studies on the photocatalytic performance and applications of HGM-TiO_2 have received limited attention.

An excellent study on the optimization of the experimental conditions to produce the highest •OH yield during photocatalysis using suspensions of Degussa P25 TiO_2 has been reported [14], but to the best of our knowledge there are no reports on optimized conditions for HGM-TiO_2 photocatalysis. The •OH generation rate is also an important parameter, since a high generation rate results in rapid degradation and short reaction times to achieve specific treatment objectives. The specific experimental conditions are critical to generation rate and yield of •OH during HGM-TiO_2 photocatalysis. For example, as the concentration of catalyst increases, the photodegradation efficiency can increase to a maximum at a specific catalyst loading above which light scattering and screening may reduce the TiO_2 photocatalytic efficiency. Terephthalic acid (TA) was employed to trap •OH effectively and selectively. Although quenching and inter filter effects may occur at high TA concentrations, these issues are not significant under dilute concentrations [15]. Another important factor is irradiation time. Since there are significant costs associated with generation of UV light, it is important to evaluate the treatment time required to achieve desired levels of degradation. From our study, •OH yield increases, whereas •OH generation rate decreases under extended irradiation time. Photocatalytic deactivation can occur when the intermediate products compete for radical species (•OH) leading to inhibition of the photocatalytic performance [16]. Therefore, it is critical to determine the optimal yield and rate of •OH generation, as a function of loading of HGM-TiO_2, concentration of TA and irradiation time.

The classical one-variable-at-a-time methodology does not enable the study of combined effects of two or more variables on a measured response. Probing each variable independently is also labor intensive and time consuming. Thus, RSM was originally developed by Box and Wilson [17], to access the interactions of various variables simultaneously and provide an empirical description of effects of variables and their interactions on a measured response. The RSM has successfully applied to determine the optimal conditions for a variety of processes [18]. Herein, RSM is used to optimize yield and average generation rate of •OH by HGM-TiO_2 photocatalysis. A central composite design was used to investigate the effects of three independent variables, namely loading of HGM-TiO_2, concentration of TA, and reaction time coded at five levels.

The RSM results were used to guide the application of HGM-TiO_2 photocatalysis in the photocatalytic degradation of DMP, as a model for problematic phthalate acid esters which have wide spread use and an annual production of approximately 4 million tons [19]. The US Environmental Protection Agency and European Union have classified these compounds as priority pollutants [20,21] because of the significant threat they pose on reproductive and behavioral health of humans and wildlife at low concentrations [22,23]. HGM-TiO_2 photocatalysis leads to the rapid destruction of DMP and there is a linear correlation between the DMP destruction and hydroxyl radical production. The results of our study demonstrate RSM can be used to readily determine the optimal conditions for hydroxyl radical production and the subsequent treatment of target compounds can be correlated to the hydroxyl radical production during HGM-TiO_2 photocatalysis.

2. Materials and methods

2.1. Chemicals

HGM-TiO_2 material was obtained from Microsphere Technology Limited (Limerick, Ireland). The characterization information of this material (including median diameter, particle size) is available from the company website http://www.microspheretechnology.com/photospheres.php.
TA (disodium salt) and DMP were purchased from Aldrich. HPLC grade methanol was obtained from Fisher. 2-Hydroxy terephthalic acid (2-HTA) was synthesized for calibration by using a published method [24]. All the chemicals were used without further purification and all solutions were made with Millipore filtered water (18 MΩ cm).

2.2. Fourier transform infrared spectroscopy (FTIR)

The TA and DMP loaded HGM-TiO_2 were prepared by adding 1.0 g HGM-TiO_2 into 100 mL solution with 1.0 g TA or DMP. The suspension was put on an orbit shaker at 300 RPM for half an hour. Solid samples for FTIR were separated, and dried in a vacuum oven at room temperature. FTIR was collected using Perkin Elmer Spectrum 100 FTIR spectrometer.

2.3. Photocatalytic and analytical methods

HGM-TiO_2 suspension was prepared by suspending HGM-TiO_2 into 100 mL TA aqueous solution in a Pyrex cylindrical reactor (12 × 1 in., ~150 mL capacity, with a vented Teflon screw top). The suspension was magnetically stirred and purged with oxygen gently for 15 min prior to radiation and during the reaction, in order to maintain the adsorption/desorption equilibrium. The suspensions were irradiated in a Rayonet photochemical reactor (Southern New England Ultra Violet Company, http://www.rayonet.org, model RPR-100), equipped with a cooling fan on the bottom and four phosphor-coated low-pressure mercury lamps (RPR 350 nm, 8.34×10^{-9} Einstein mL^{-1} s^{-1}). Samples (3 mL) were taken from the suspension at given time intervals and immediately filtered through a 0.45 μm PTFE filter to remove suspended particles prior to analysis.

TA is used to selectively trap •OH and to produce 2-HTA with a percent yield of 35% [25] (Scheme 1). The yield of •OH is quantified by fluorescent measurement of the generated 2-HTA. 2-HTA was excited at 315 nm to emit fluorescence at 425 nm [26], which was measured on a Horiba FluoroMax 3 spectrofluorometer.

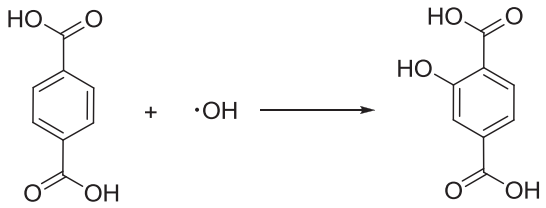

Scheme 1. Reaction of TA with •OH.

Table 1
Central composite design for RSM.

Experiment entry	Variable in coded levels		
	x_1	x_2	x_3
1	−1	−1	−1
2	−1	−1	1
3	−1	1	−1
4	−1	1	1
5	1	1	1
6	1	1	−1
7	1	−1	1
8	1	−1	−1
9	0	0	α
10	0	0	$-\alpha$
11	0	α	0
12	0	$-\alpha$	0
13	α	0	0
14	α	0	0
15	0	0	0
16	0	0	0
17	0	0	0
18	0	0	0
19	0	0	0
20	0	0	0

2.4. Experimental design and data analysis

To identify best combination of experimental parameters for optimal •OH generation, RSM was applied. Central composite design was employed for the optimal conditions. A full factorial 5-level experimental design with 3 variables needs to run $5^3 = 125$ experiments. However, as shown in Table 1, application of the central composite design reduces the number of required experiments to 20 (8 factor points, 6 axial points and 6 replications at the center points) [27]. Alpha (α) is the coded level of axial point from the center. The coded level is (x_i) defined by the following equation:

$$x_i = \frac{X_i - X_0}{\Delta X_i} \quad (9)$$

where X_0 is the real value of the independent variable at the center point, X_i is the real value of the independent variable, and ΔX_i is the step changing value.

In this study, the loading of HGM-TiO_2 (X_1), TA concentration (X_2) and irradiation time (X_3) were varied. The real levels and coded levels are showed in Table 2. The equation can quantitatively describe the predicted response as a function of three variables and the optima of three variables are obtained by surface response. Herein, Y is the yield of •OH or its average generation rate, which is

Table 2
Real and coded levels of three variables.

Variable	Symbol coded	Coded level				
		$-\alpha$ (−2)	−1	0	1	α (2)
[HGM-TiO_2] (g/L)	X_1	2	4	6	8	10
[TA] (mM)	X_2	1	2	3	4	5
Irradiation time (min)	X_3	5	10	15	20	25

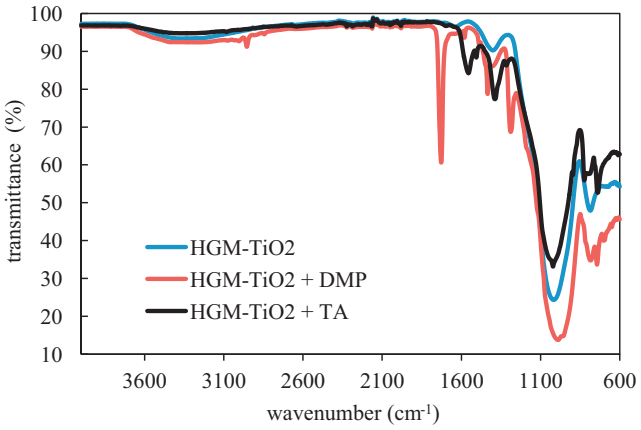

Fig. 1. FTIR spectra of HGM-TiO_2, TA- and DMP-loaded onto HGM-TiO_2.

defined by the following equation:

$$Y = b_0 = b_1X_1 = b_2X_2 + b_3X_3 + b_{12}X_1X_2 + b_{13}X_1X_3 + b_{23}X_2X_3 + b_{11}X_1^2 + b_{22}X_2^2 + b_{33}X_3^2 \quad (10)$$

where Y is the predicted response, b_0 is the intercept, b_1, b_2 and b_3 are linear coefficients, b_{12}, b_{13} and b_{23} are squared coefficients, b_{11}, b_{22} and b_{33} are quadratic coefficients.

2.5. Degradation and analysis of DMP

The optimal conditions for the generation of •OH were employed for degradation of DMP. The concentration of DMP residual was analyzed using a Varian ProStar HPLC system equipped with a ProStar 410 autosampler and a ProStar 335 photodiode array detector with the stationary phase being a Luna RP C18 column of 250 mm × 4.6 mm I.D. (5 μm particle size). The mobile phase consisted of a mixture of water (50%) and methanol (50%), and detection wavelength was 230 nm. The flow rate was 1 mL min^{-1} and the injection volume is 30 μL at room temperature [28]. The retention time of DMP is ~12.2 min under these HPLC conditions.

3. Results and discussion

3.1. FTIR

The FTIR spectra of were recorded in the range 600–4000 cm^{-1} to identify the functional groups of HGM-TiO_2 and access the adsorption of TA and DMP onto HGM-TiO_2 (Fig. 1). For the neat HGM-TiO_2 sample, the infrared band at 3374 cm^{-1} shows the presence of OH stretching vibration [29], while the IR band at 1631 cm^{-1} is ascribed to Si—H_2O adsorption [30,31]. The peak at 1404 cm^{-1} corresponds to O—H bending mode [32], the band at 1019 cm^{-1} corresponds to Si—OH and Si—O—Ti vibration modes [33] while a Ti—O—Ti band appears at 787 cm^{-1}. These assignments clearly demonstrate the HGM-TiO_2 contains characteristic bands associated with TiO_2 and glass [34]. The DMP loaded HGM-TiO_2 materials exhibit a band at 2954 cm^{-1} corresponding to $C_{(sp3)}$—H stretching [35], a band at 1727 cm^{-1} is assigned to C=O stretching [36], a C—O stretching band at 1289 cm^{-1}, a band at 743 cm^{-1} indicative of ortho-disubstituted benzene ring [37] and a band at 1434 cm^{-1} is assigned to C—H group [38]. For TA loaded HGM-TiO_2, the band at 1555 cm^{-1} corresponds to antisymmetric —CO_2 stretching [39], the band at 823 cm^{-1} is ascribed to =C—H bending of an aromatic ring [40]. The remaining bands are ascribed to HGM-TiO_2. The results demonstrate adsorption of DMP and TA onto the HGM-TiO_2 materials.

Table 3
RSM central composite design and experimental and expected responses.

X_1	X_2	X_3	Experimental Y_1	Predicted Y_1	Experimental Y_2	Predicted Y_2
6	3	5	95.8	99.4	19.17	18.28
6	3	15	176.7	176.5	11.78	11.80
6	3	25	228.2	221.6	9.13	9.73
2	3	15	108.0	114.1	7.20	7.39
10	3	15	202.1	192.4	13.47	13.02
6	1	15	115.0	114.7	7.67	7.63
6	5	15	174.4	171.1	11.63	11.34
4	2	10	107.0	103.1	10.70	11.11
4	2	20	152.0	152.1	7.60	7.36
8	2	10	131.5	133.3	13.15	14.08
8	2	20	178.0	188.3	8.90	9.25
4	4	10	120.9	116.3	12.09	12.57
4	4	20	179.5	183.5	8.97	8.85
8	4	10	152.6	158.3	15.26	16.30
8	4	20	221.9	231.5	11.09	11.50
6	3	15	175.9	176.5	11.72	11.80
6	3	15	177.4	176.5	11.83	11.80
6	3	15	176.9	176.5	11.79	11.80
6	3	15	176.0	176.5	11.73	11.80
6	3	15	177.5	176.5	11.83	11.80

3.2. Model fitting and 3D response surface

The data of •OH yield and average rate of •OH generation are shown in Table 3. The experimental data were fitted to empirical second-order polynomial models by a regression function in Microsoft Excel 2007. The results indicate that the experimental and expected responses match well, and the experimental responses fit the second-order polynomials well. The empirical second-order polynomials were obtained as the following two equations:

$$Y_1 = -98.78 + 20.49X_1 + 41.91X_2 + 7.28X_3 + 1.48X_1X_2 + 0.15X_1X_3 + 0.91X_2X_3 = 1.45X_1^2 - 8.39X_2^2 - 0.16X_3^2 \quad (11)$$

$$Y_2 = 6.71 + 2.02X_1 + 3.81X_2 - 0.93X_3 + 0.096X_1X_2 - 0.027X_1X_3 + 0.0015X_2X_3 - 0.10X_1^2 - 0.58X_2^2 + 0.022X_3^2 \quad (12)$$

where Y_1 is the predicted response of yield of generated •OH (μM), Y_2 is the predicted average generation rate of •OH (μM/min), the variables of X_1, X_2 and X_3 are the loading of HGM-TiO_2 (g/L), concentration of TA (mM) and irradiation time (min), respectively.

In order to check the adequacy of the second-order models, the significance test and analysis of variance (ANOVA) were employed for the second-order models for •OH yield and the average •OH generation rate. The significance tests of estimated regression coefficients for •OH yield and average •OH generation rate are shown in Table 4. The probability value (P) of coefficients was greater than 0.05, indicating the term did not have a significant effect on the predicted response. Otherwise, it was rejected and this term influenced the predicted response at a significant confidence level. For Eqs. (11) and (12), X_1, X_2, X_3, X_1X_1, X_2X_2 and X_3X_3 were significant terms for the predicted response, and X_1X_2, X_1X_3 and X_2X_3 were insignificant terms. The determination coefficient (R^2) for •OH yield was calculated as 0.982, which can explain the variability of response at a 0.982 confidence level. Moreover, the adjusted R^2 value of 0.966 was also close to 1. For Y_2, R^2 was 0.974 and adjusted R^2 was 0.951. Therefore, as well as the model for •OH yield, the predicted values had a good agreement with experimental data.

Table 4
Estimated regression coefficients for •OH yield and the average •OH generation rate.

Term	•OH yield			Average •OH generation rate		
	Coefficient	Std. error	P	Coefficient	Std. error	P
X_1	20.49	6.71	0.012	2.02	0.60	0.007
X_2	41.91	13.43	0.011	3.81	1.19	0.010
X_3	7.28	2.69	0.022	−0.93	0.24	0.003
X_1X_2	1.48	1.23	0.256	0.096	0.11	0.398
X_1X_3	0.15	0.24	0.550	−0.027	0.022	0.236
X_2X_3	0.91	0.49	0.093	0.0015	0.044	0.973
X_1X_1	−1.45	0.35	0.002	−0.10	0.031	0.008
X_2X_2	−8.39	1.38	0.000	−0.58	0.12	0.001
X_3X_3	−0.16	0.055	0.015	0.022	0.0049	0.001

The response surface models were further analyzed by ANOVA and the output results are summarized in Table 5. The P value of regression model was less than 0.05, so the models were adequate to describe the variability of Y_1 and Y_2 as a function of X_1, X_2 and X_3. The linear and square effects were highly significant for the predicted responses, whereas the interaction effects were insignificant. In conclusion, both Eqs. (11) and (12) are good approximations.

To obtain the optimal conditions for •OH generation, the 3D response surface technique was employed to evaluate the effects of independent variables on Y_1 and Y_2. Fig. 2 shows the effect of any two independent variables on the •OH yield and its average •OH generation rate, keeping the coded level of the third one at its central level (0).

Fig. 2a, c, d and f demonstrates the effect of concentration of TA on Y_1 and Y_2. Y_1 and Y_2 increase with increase in concentration of TA until Y_1 and Y_2 reach a highest value. The optimal value of concentration of TA for Y_1 and Y_2 is 4.0 mM. The effect of loading of HGM-TiO_2 on Y_1 and Y_2 is shown in Fig. 2b, c, e and f. The optimal value of concentration of HGM-TiO_2 on Y_1 and Y_2 is 8.0 g/L. Fig. 2a, b, d and e demonstrates the effect of irradiation time on Y_1 and Y_2. •OH yield increases whereas the average •OH generation rate decreases with increase in irradiation time. The competition for hydroxyl radical between TA and the oxidation products and TA consumption are factors leading to the observed decrease in •OH generation rate. Although the overall •OH yields increase with irradiation time, the rate of •OH yield slowed significantly after 20 min. Thus, the optimal time for Y_1 and Y_2 is 20 min. In summary, the optimal conditions for the yield of •OH were 8.0 g/L HGM-TiO_2, 4.0 mM TA and 20 min for irradiation time.

3.3. The degradation of DMP

The optimal conditions for the •OH generation were applied for the degradation of DMP. The initial concentration of DMP is 50 μM. The loss of DMP follows the pseudo-first order kinetic model. The pseudo-first order kinetic model can be expressed as [41]:

$$\frac{d[C]}{dt} = -k[C] \quad (13)$$

After definite integration, the equation becomes

$$ln\left(\frac{C_0}{C}\right) = kt \quad (14)$$

where k is the rate constant of pseudo-first order model (min^{-1}), t is time (min), C_0 is the initial concentration of DMP (μM) and C is the concentration of DMP (μM) at the specific time. Since R^2 of plot of $\ln C_0/C$ versus t is greater than 0.95, the experimental data fit the pseudo-first-order model nicely.

As shown in Fig. 3, the rate constants for degradation of DMP increased with increase in loading of HGM-TiO_2, and reached the highest at 8.0 g/L HGM-TiO_2. No significant increase is observed at loading levels above 8.0 g/L HGM-TiO_2. At high loadings of HGM-TiO_2 (>8.0 g/L), the rate does not change but the standard deviation becomes larger due to the light scattering and screening effects. Therefore, the loading of HGM-TiO_2 = 8.0 g/L was considered optimal. In order to assess the relationship between •OH yield and

Table 5
ANOVA for the second-order models of •OH yield and average •OH generation rate.

Source	•OH yield				Average •OH generation rate			
	DF[a]	Sum of squares	*F*	*P*	DF	Sum of squares	*F*	*P*
Regression	9	26446.4	60.99	0.000	9	144.03	42.08	0.000
Linear	3	23932.0	5.02	0.022	3	118.47	19.02	0.000
Square	3	2260.3	15.64	0.000	3	24.65	21.61	0.000
Interaction	3	254.0	1.76	0.219	3	0.90	0.79	0.526
Residual error	10	481.8			10	3.80		
Total	19	26928.2			19	147.83		

[a] DF is degree of freedom.

degradation of DMP, the plot of degraded DMP against •OH yield is demonstrated in Fig. 4. The •OH yield derived from Eq. (11) with the coded level of X_2 at the central level (0) and X_3 being 20 min, showing increased •OH yield as the increasing of loading of HGM-TiO_2 (2–10 g/L). After 20 min, DMP was eliminated in presence of ≥8.0 g/L HGM-TiO_2, in agreement with the optimal conditions of •OH generation. The linear relationship between •OH yield and DMP degradation indicates the •OH is responsible for degradation of DMP. The bimolecular reaction rate constants for the reaction of •OH with TA is 3.3×10^9 M^{-1} s^{-1} [42], while it is 4×10^9 M^{-1} s^{-1} for DMP [43]. The rate constants are similar; however the trend-line in Fig. 4 demonstrates the destruction of DMP correlates to the •OH yield, but not in a 1:1 ratio. The yield of •OH and TA adduct versus destruction of DMP may be related to the different adsorption properties of DMP versus TA on HGM-TiO_2. Since •OH is a relatively nonselective radical and is able to react with substance at nearly diffusion controlled rate, the oxidation products of DMP may be degraded further before they are released back to aqueous phase.

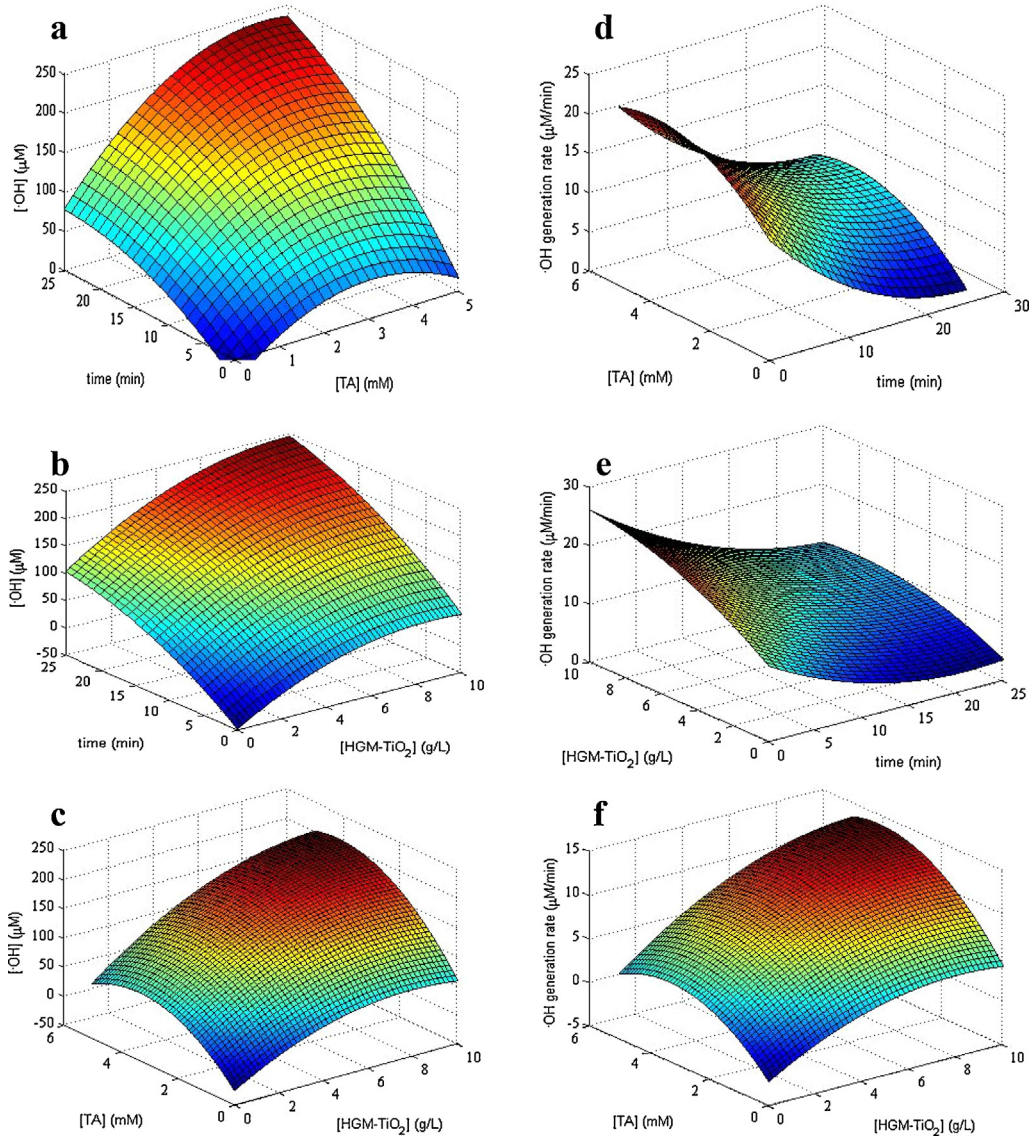

Fig. 2. Response surface showing of any two independent variables on the •OH yield (a–c) and its average •OH generation rate (d–f).

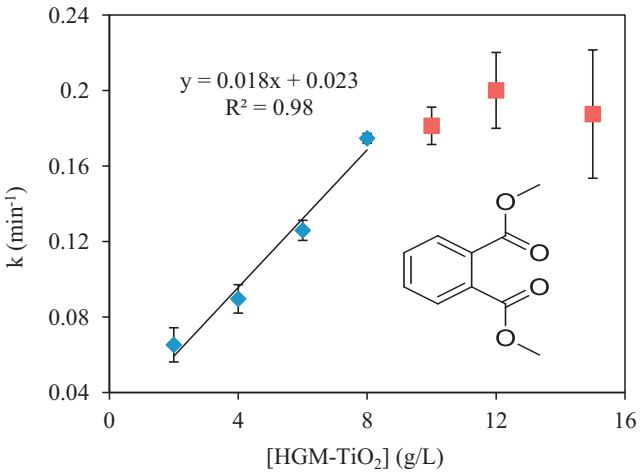

Fig. 3. The rate constants of pseudo-first order kinetic model for degradation of DMP as a function of HGM-TiO_2 loading. The data at 10, 12 and 15 g/L were not used for the trend-line since the rate did not increase above 8.0 g/L. Error bars represent standard deviation of triplicate experiments. The insert is the molecular structure of DMP.

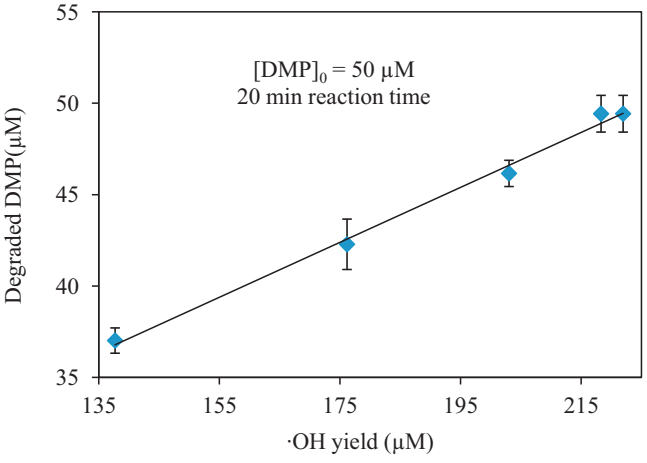

Fig. 4. Plot of degraded DMP against •OH yield. Error bars represent standard deviation of triplicate experiments.

4. Conclusions

The FTIR spectra show that the HGM-TiO_2 exhibits adsorption of TA (•OH trap) and DMP (target compound). The loading of HGM-TiO_2, the concentration of TA and irradiation time affect •OH generation significantly. The optimum conditions of •OH generation by HGM-TiO_2 were measured using RSM. Statistical analyses indicate the empirical second-order polynomials can accurately describe the •OH yield and the average •OH generation rate. The 3D response surface graphs showed that the optimum conditions of loading of HGM-TiO_2, concentration of TA and irradiation time were 8.0 g/L, 4.0 mM, and 20 min, respectively. The optimal condition for •OH generation by HGM-TiO_2 has applied to the degradation of DMP. The degradation of DMP follows the pseudo-first order kinetic model nicely, and rate constant increased linearly as increasing of loading of HGM-TiO_2 up to 8.0 g/L. We have demonstrated RSM can be used to determine the optimal conditions for •OH generation. Employing the optimal conditions, the problematic pollutant, DMP, is readily degraded. The effective application of RSM for determining optimal conditions for hydroxyl radical production and rapid destruction of DMP show HGM-TiO_2 photocatalysis is a promising material for water treatment.

Acknowledgement

K.E.O. and D.D.D. gratefully acknowledge NSF support (CBET, award 1033317).

References

[1] E.K. O'Shea, D.D. Dionysiou, Advanced oxidation processes for water treatment, Journal of Physical Chemistry Letters 3 (2012) 2112–2113.
[2] M.R. Hoffmann, S.T. Martin, W. Choi, D.W. Bahnemann, Environmental application of semiconductor photocatalysis, Chemical Reviews 95 (1995) 69–96.
[3] M.A. Fox, M.T. Dulay, Heterogeneous photocatalysis, Chemical Reviews 93 (1993) 341–357.
[4] A.L. Linsebigler, G. Lu, J.T. Yates, Photocatalysis on TiO_2 surfaces: principles, mechanisms, and selected results, Chemical Reviews 95 (1995) 735–758.
[5] U. Khan, N. Benabderrazik, A.J. Bourdelais, D.G. Baden, K. Rein, P.R. Gardinali, L. Arroyo, K.E. O'Shea, UV and solar TiO_2 photocatalysis of brevetoxins (PbTxs), Toxicon 55 (2010) 1008–1016.
[6] G.V. Buxton, C.L. Greenstock, W.P. Helman, A.B. Ross, Critical review of rate constants for reactions of hydrated electrons, hydrogen atoms and hydroxyl radicals (•OH/•O^-) in aqueous solution, Journal of Physical and Chemical Reference Data 17 (1988) 513–886.
[7] Y. Kado, R. Hahn, P. Schmuki, Surface modification of TiO_2 nanotubes by low temperature thermal treatment in C_2H_2 atmosphere, Journal of Electroanalytical Chemistry 662 (2011) 25–29.
[8] C. Yogi, K. Kojima, N. Wada, H. Tokumoto, T. Takai, T. Mizoguchi, H. Tamiaki, Photocatalytic degradation of methylene blue by TiO_2 film and Au particles-TiO_2 composite film, Thin Solid Flims 516 (2008) 5881–5884.
[9] D. Graham, H. Kisch, L.A. Lawson, P.K.J. Robertson, The degradation of microcystin-LR using doped visible light absorbing photocatalysts, Chemosphere 78 (2010) 1182–1185.
[10] Z. Liu, X. Zhang, S. Nishimoto, M. Jin, D.A. Tryk, T. Murakami, A. Fujishima, Highly ordered TiO_2 nanotube arrays with controllable length for photoelectrocatalytic degradation of phenol, Journal of Physical Chemistry C 112 (2008) 253–259.
[11] C. Wang, X. Zhang, H. Liu, X. Li, W. Li, H. Xu, Reaction kinetics of photocatalytic degradation of sulfosalicylic acid using TiO_2 microspheres, Journal of Hazardous Materials 163 (2009) 1101–1106.
[12] G. Li, R. Bai, X.S. Zhao, Coating of TiO_2 thin films on the surface of SiO_2 microspheres: toward industrial photocatalysis, Industrial and Engineering Chemistry Research 47 (2008) 8228–8232.
[13] N.B. Jackson, C.M. Wang, Z. Luo, J. Schwitzgebel, J.G. Ekerdt, J.R. Brock, A. Heller, Attachment of TiO_2 powders to hollow glass microbeads: activity of the TiO_2-coated beads in the photoassisted oxidation of ethanol to acetaldehyde, Journal of the Electrochemical Society 138 (1991) 3660–3664.
[14] S.A.V. Eremia, D. Chevalier-Lucia, G. Radu, J. Marty, Optimization of hydroxyl radical formation using TiO_2 as photocatalyst by response surface methodology, Talanta 77 (2008) 858–862.
[15] K. Ishibashi, A. Fujishima, T. Watanabe, K. Hashimoto, Detection of active oxidative species in TiO_2 photocatalysis using the fluorescence technique, Electrochemistry Communications 2 (2000) 207–210.
[16] L. Cao, Z. Gao, S.L. Suib, T.N. Obee, S.O. Hay, J.D. Freihaut, Photocatalytic oxidation of toluene on nanoscale TiO_2 catalysts: studies of deactivation and regeneration, Journal of Catalysis 196 (2000) 253–261.
[17] G.E.P. Box, K.B. Wilson, On the experimental attainment of optimum conditions, Journal of the Royal Statistical Society 13 (1951) 1–45.
[18] I. Arslan-Alaton, G. Tureli, T. Olmez-Hanci, Treatment of azo dye production wastewaters using Photo-Fenton-like advancedoxidation processes: optimization by response surface methodology, Journal of Photochemistry and Photobiology A 202 (2009) 142–153.
[19] Z.-P. Lin, M.G. Ikonomou, H. Jing, C. Mackintosh, F.A.P.C. Gobas, Determination of phthalate ester congeners and mixtures by LC/ESI-MS in sediments and biota of an urbanized marine inlet, Environmental Science and Technology 37 (2003) 2100–2108.
[20] US Environmental Protection Agency (US EPA), National Primary Drinking Water Regulation: Federal Register, 40 CFR, Part 141, Washington, DC, July 1, 1991 (Chapter I).
[21] B.G. Hansen, A.G. van Haelst, K. van Leeuwen, P. van der Zandt, Priority setting for existing chemicals: European Union risk ranking method, Environmental Toxicology and Chemistry 18 (1999) 772–779.
[22] M. Matsumoto, M. Hirata-Koizumi, M. Ema, Potential adverse effects of phthalic acid esters on human health: a review of recent studies on reproduction, Regulatory Toxicology and Pharmacology 50 (2008) 37–49.
[23] J.A. Dean, Lange's Handbook of Chemistry (eBook), 15th ed., McGraw-Hill, New York, 1999.
[24] T.J. Mason, J.P. Lorimer, D.M. Bates, Y. Zhao, Dosimetry in sonochemistry: the use of aqueous terephthalate ion as a fluorescence monitor, Ultrasonics Sonochemistry 1 (1994) S91–S95.
[25] X. Fang, G. Mark, C. von Sonntag, OH radical formation by ultrasound in aqueous solutions. Part I: the chemistry underlying the terephthalate dosimeter, Ultrasonics Sonochemistry 3 (1996) 57–63.
[26] K. Ishibashi, A. Fujishima, T. Watanabe, K. Hashimoto, Quantum yields of active oxidative species formed on TiO_2 photocatalyst, Journal of Photochemistry and Photobiology A 134 (2000) 139–142.

[27] N.B. Parilti, C.S.U. Demirel, M. Bekbolet, Response surface methodological approach for the assessment of the photocatalytic degradation of NOM, Journal of Photochemistry and Photobiology A 225 (2011) 26–35.
[28] Y. Chen, L. Chen, N. Shang, Photocatalytic degradation of dimethyl phthalate in an aqueous solution with Pt-doped TiO_2 coated magnetic PMMA microspheres, Journal of Hazardous Materials 172 (2009) 20–29.
[29] M. Burgos, M. Langlet, The sol–gel transformation of TIPT coating: a FTIR study, Thin Solid Films 349 (1999) 19–23.
[30] J. Wang, T. Ma, Z. Zhang, X. Zhang, Y. Jiang, W. Sun, R. Li, P. Zhang, Investigation on the transition crystal of ordinary rutile TiO_2 powder by microwave irradiation in hydrogen peroxide solution and its sonocatalytic activity, Ultrasonics Sonochemistry 14 (2007) 575–582.
[31] B. Ding, H. Kim, C. Kim, M. Khil, S. Park, Morphology and crystalline phase study of electrospun TiO_2–SiO_2 nanofibres, Nanotechnology 14 (2003) 532–537.
[32] B.P. Singh, S. Nayak, S. Samal, S. Bhattacharjee, L. Besra, The role of poly(methacrylic acid) conformation on dispersion behavior of nano TiO_2 powder, Applied Surface Science 258 (2012) 3524–3531.
[33] J. Zhai, T. Yang, L. Zhang, X. Yao, The optical waveguiding properties of TiO_2–SiO_2 composite films prepared by the sol–gel process, Ceramics International 25 (1999) 667–670.
[34] M. Minella, M.G. Faga, V. Maurino, C. Minero, E. Pelizzetti, S. Coluccia, G. Martra, Effect of fluorination on the surface properties of titania P25 powder: an FTIR study, Langmuir 26 (2010) 2521–2527.
[35] J. Ibarra, E. Muñoz, R. Moliner, FTIR study of the evolution of coal structure during the coalification process, Organic Geochemistry 24 (1996) 725–735.
[36] B.N. Khare, M. Meyyappan, A.M. Cassell, C.V. Nguyen, J. Han, Functionalization of carbon nanotubes using atomic hydrogen from a glow discharge, Nano Letters 2 (2002) 73–77.
[37] C.F. Liu, R.C. Sun, J. Ye, Structural and thermal characterization of sugarcane Bagasse phthalates prepared with ultrasound irradiation, Polymer Degradation and Stability 91 (2006) 280–288.
[38] L.M. Matuana, D.P. Kamdem, J. Zhang, Photoaging and stabilization of rigid PVC/wood–fiber composites, Journal of Applied Polymer Science 80 (2001) 1943–1950.
[39] L. Liao, C. Lien, D. Shieh, M. Chen, J. Lin, FTIR study of adsorption and photoassisted oxygen isotopic exchange of carbon monoxide, carbon dioxide, carbonate, and formate on TiO_2, Journal of Physical Chemistry B 106 (2002) 11240–11245.
[40] D.L. Pavia, G.M. Lampman, G.S. Kriz, J.A. Vyvyan, Introduction to Spectroscopy, 4th ed., Brooks/Cole, Belmont, CA, 2009.
[41] S. Ye, Q. Tian, X. Song, S. Luo, Photoelectrocatalytic degradation of ethylene by a combination of TiO_2 and activated carbon felts, Journal of Photochemistry and Photobiology A 208 (2009) 27–35.
[42] W. Song, S. Yan, W.J. Cooper, D.D. Dionysiou, K.E. O'Shea, Hydroxyl radical oxidation of cylindrospermopsin (cyanobacterial toxin) and its role in the photochemical transformation, Environmental Science and Technology 46 (2012) 12608–12615.
[43] W.R. Haag, C.C.D. Yao, Rate constants for reaction of hydroxyl radical with several drinking water contaminants, Environmental Science and Technology 26 (1992) 1005–1013.